DIRECT NUMERICAL SIMULATION OF THREE-DIMENSIONAL FLOW PAST A YAWED SQUARE CYLINDER

Lou X., Zhou T.*, Jiang H. and Cheng L.
*Author for correspondence
School of Civil, Environmental and Mining Engineering,
The University of Western Australia, WA6009, Australia,
E-mail: tongming.zhou@uwa.edu.au

ABSTRACT

Direct numerical simulations (DNS) of flow past a stationary square cylinder with yaw angles of 0°~45° are performed at Reynolds number of 1000. The three-dimensional Navier-Stokes equations are solved using the finite volume method with OpenFOAM. The effect of yaw angles on the wake structures is investigated in terms of the vortex shedding frequency, hydrodynamic forces and vorticity iso-contours. Significant changes in the flow field can be observed when the yaw angle increases from 0° to 45°. The appearance of the spanwise velocity component and the less organized spanwise vorticity contour at large yaw angles denote the impairment of the quasi-two-dimensionality and the development of the three-dimensionality of the wake.

INTRODUCTION

When a steady current passes a cylinder at a yaw angle α (the angle between the flow direction and the plane perpendicular to the cylinder axis), the fluid velocity component in the cylinder axial direction may play an important role in the vortex formation and the existence of yaw angle would intensify the three-dimensional effect of the wake flow. In practical engineering applications, to simplify the analysis, normally only the velocity component perpendicular to the cylinder axis is used to quantify the hydrodynamic forces and vortex shedding frequency of the cylinder. This is the so-called independence principle (IP), or the cross flow principle or the cosine law. For a yawed circular cylinder, the validity of IP in steady current has been investigated both experimentally [1-3] and numerically [4, 5], even though there are some discrepancies with the angle range over which the IP is valid. Generally the consensus maximum yaw angle within which the IP is valid is about 40°~45°.

With increasing use of square-cross-section slender structures in engineering, extensive studies on flow and force characteristics of the square cylinder wake have been conducted [6-8]. Though the near wake structures of both the circular and square cylinders are expected to be topologically similar to one another, at high Reynolds numbers ($Re = U_\infty D/\nu$, where U_∞ is the free stream velocity, D is the side length of the square cylinder and ν is the kinematic viscosity of the fluid), the sharp corners of the square cylinder may significantly affect the evolution of the wake flow. The numerical simulation has been proved to be an effective way to study the wake characteristics of a cylindrical body. It is found by [7] that for a square cylinder at *Re* of about 175, the three-dimensional structure is formed with intermittent large-scale irregularities as a result of vortex merging in the spanwise direction or due to the phase variations within the large coherent structures. The values of the Strouhal number and the time-averaged drag coefficient are closely associated with each other over a given range of *Re* (150~500), reflecting the spatial structure of the wake. Based on the investigation the turbulent flow past a square cylinder confined in a channel at $Re = 3900$ with large eddy simulation [9], one pair of extra recirculation regions are observed near the upper and lower faces of the square cylinder, which is absent from the flow past a circular cylinder. They found that the recirculation region behind the cylinder is reduced by the channel walls, which results in the larger drag forces, higher lift fluctuations and Strouhal number than those of the infinite domain case. In order to examine the effect of corner shapes on the dynamic pressures of a square cylinder, the three-dimensional flows around square cylinders with sharp, chamfered and rounded corners was simulated using the direct finite difference scheme at $Re = 10000$ [10]. It was found that the dynamic forces undergo a drastic modification (as much to 60%) when the corner shape is slightly changed. The changes mainly result from the narrower separating shear layers for the modified square shape.

Apart from the studies mentioned above, our knowledge about the effect of cylinder yaw angle on vortical structures and hydrodynamic forces of a square cylinder wake is still limited. In this paper, we aim to investigate the vortical structures of an infinitely long square cylinder in steady flow with yaw angles of 0°, 15°, 30° and 45° by solving the Navier-Stokes equations numerically at $Re = 1000$. The effect of the yaw angle on the wake flow of a square cylinder was examined in terms of the force coefficients, the vortex shedding frequency as well as the vortex flow structures.

NUMERICAL METHOD

The 3D Navier-Stokes (NS) equations and the continuity equation are used as the governing equations, which are expressed as

$$\frac{\partial u_i}{\partial t} + u_j \frac{\partial u_i}{\partial x_j} + \frac{\partial p}{\partial x_i} - \frac{1}{Re}\frac{\partial^2 u_i}{\partial x_j^2} = 0 \quad (1)$$

$$\frac{\partial u_i}{\partial x_j} = 0 \quad (2)$$

where x_i, x_j and x_k refer to the streamwise (x), transverse (y) and spanwise (z) direction, respectively (as defined in Figure

1), u_i is the fluid velocity component in the x_i direction, and p is the pressure. The NS equations are solved by the Open source Field Operation and Manipulation (OpenFOAM®) C++ libraries which used the finite volume method (FVM) in the solver and the pressure-velocity coupling is based on the pressure implicit with splitting of operators (PISO) method. The convection term is discretized using the Gauss cubic scheme, and the diffusion term is discretized using the Gauss linear scheme. The Euler implicit scheme is adopted for the temporal discretization.

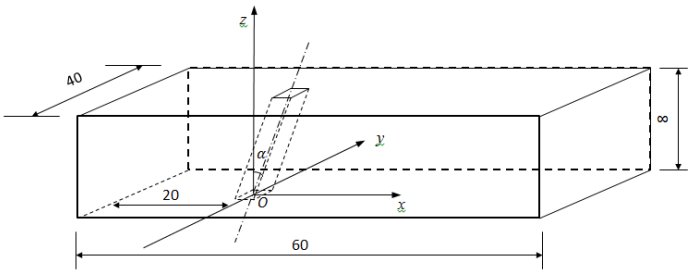

Figure 1 Schematic plot of the coordinate and the computational domain (Unit: *D*)

Figure 1 shows the non-dimensional rectangular computational domain with $60D \times 40D \times 8D$ in the streamwise, transverse and spanwise direction, respectively. The periodic boundary condition is applied for the top and bottom boundaries, and the symmetric boundary condition is adopted for the left and right boundaries which are parallel to the cylinder axis. The initial velocity at the inlet boundary is set to be zero and the outlet boundary is set to be zero-gradient. A reference pressure of zero is applied at the outlet boundary. Around the cylinder surface the no-slip boundary condition is applied as the non-slip wall and periodic boundary conditions can significantly reduce the effect of the spanwise walls on the three-dimensionality of the flow around a yawed cylinder. The computations were performed on a cluster of computers located in the Pawsey Supercomputing Center, Western Australia. The simulations were carried out up to the fully developed vortex shedding process has occurred for at least 10 cycles.

MESH DEPENDENCE CHECK

A 2D mesh is generated in the (*x*, *y*)-plane with high mesh resolution close to the cylinder and even higher resolution at the tips of the cylinder. High resolution mesh is also applied downstream the cylinder up to $x = 10D$ so that more information of the velocity and vorticity variations can be resolved. The 2D mesh is then extended in the *z*-direction with certain layers to obtain the 3D mesh. Two kinds of meshes were applied first to investigate the mesh dependence for $\alpha = 0°$, i.e. the coarse and the fine meshes. The results (drag coefficient and Strouhal number) can also be used as a validation of the present numerical methods when compared with those obtained previously. Table 1 lists the mesh characteristics, mean drag coefficient $\bar{C}_D$ ($\equiv F_D/(1/2\rho U_\infty^2 D)$, where F_D is the drag force in *x*-direction and ρ is the density of the fluid, the RMS values of the lift coefficient C_{Lrms} ($\equiv F_{Lrms}/(1/2\rho U_\infty^2 D)$, where F_{Lrms} is the RMS values of the lift force in *y*-direction and the Strouhal number St ($\equiv f_0 D/U_\infty$), where f_0 is the vortex shedding frequency obtained from the two kinds of meshes. Both drag and lift forces are calculated by integrating the pressure and the shear stress around the whole cylinder surface.

Table 1 Mesh dependence check for $\alpha = 0°$ at $Re = 1000$

Mesh density	Coarse	Fine
Node number	1029530	2376640
Node number along cylinder circumstance	136	200
Node number along cylinder length	80	80
Mesh size next to the cylinder surface (Unit: *D*)	0.00734	0.00503
Mean drag coefficient $\bar{C}_D$	2.11	2.13
RMS value of lift coefficient C_{Lrms}	1.52	1.50
Strouhal number St	0.124	0.121

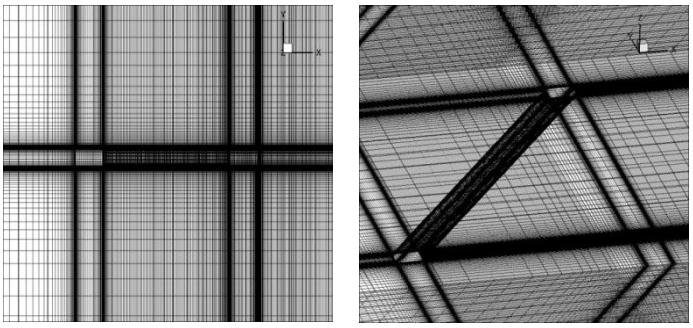

Figure 2 Schematic plots of the computational mesh viewed from different planes for $\alpha = 45°$

The mean drag coefficient $\bar{C}_D$ for both the fine mesh (2.13) and the coarse mesh (2.11) are in accordance with the experimental results of 2.2 by [11], 2.15 by [12], and the numerical result of 1.97 by [9]. The Strouhal number for the fine and coarse meshes are 0.121 and 0.124, respectively, which are in good agreement with the experimental results between 0.12 and 0.125 by [12], 0.127 by [13] and the numerical result of 0.125 by [9]. According to Table 1, one can notice that the differences in the mean drag coefficient, Strouhal number and RMS value of the lift coefficient between the fine mesh and the coarse mesh are about 1.1%, 1.7% and 2.2%, respectively. Therefore, to reduce the calculation time, the coarse mesh is applied for all the yaw angles with the same density. Figure 2 demonstrates the schematic plots of the meshes employed in the present study for $\alpha = 45°$.

RESULTS AND DISCUSSION

Force Coefficients and Vortex Shedding Frequency

The mean drag coefficient $\bar{C}_D$ among different angles varies from 2.107 to 1.969, 1.596 and 1.086 as α changes from 0° to 15°, 30° and 45°, respectively. However, when the velocity component normal to the cylinder axis U_N ($\equiv U_\infty \cos\alpha$) is used in the calculation of $\bar{C}_D$, the values of $\bar{C}_{DN}$ ($= F_D/(1/2\rho U_N^2 D)$ are 2.110, 2.128 and 2.172 for $\alpha =$ 15°, 30° and 45°, respectively. Compared with that of $\alpha = 0°$, the deviation is within 3% for the normalized mean drag coefficient at $\alpha = 45°$, indicating the validity of IP.

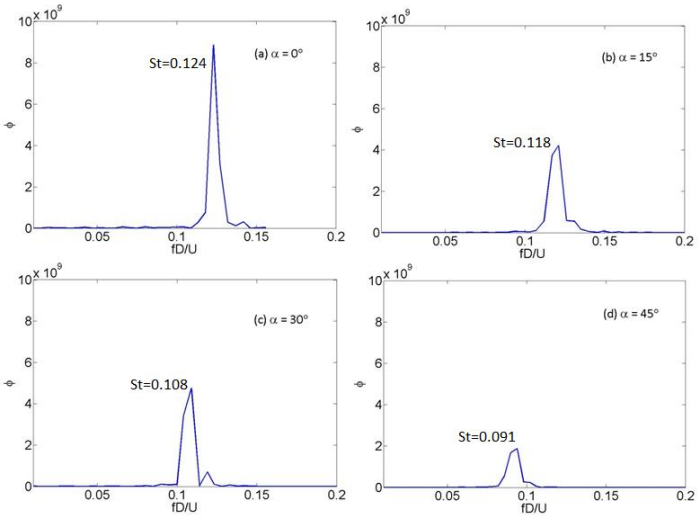

Figure 3 Energy spectrum of transverse velocity v for different angles

To verify the IP in terms of vortex shedding frequency, the spectra of the transverse velocity v on the wake centerline for different cylinder yaw angles are shown in Figure 3. The power spectral density functions ϕ is defined as $\int_0^\infty \phi(x)\,dx = v^2$, which is obtained by calculating FFT (Fast Fourier Transform) of the velocity signals. The horizontal axis is normalized by D and U so that the peak location corresponds to the Strouhal number. The spectra at different yaw angles all display a pronounced peak, indicating the apparent vortex shedding. With the increase of the yaw angle, the Strouhal number decreases from 0.124 at $\alpha = 0°$ to 0.118, 0.108 and 0.091 at $\alpha =$ 15°, 30° and 45°, respectively. Similar to the drag coefficient, if the vortex shedding frequency is normalized by U_N, the corresponding normalized Strouhal number (St_N) for $\alpha =$ 15°, 30° and 45° is 0.122, 0.125 and 0.128, respectively. The 3% deviation in St_N at $\alpha = 45°$ from that of $\alpha = 0°$ supports the application of the IP for yaw angles up to 45°. In addition, the energy of the peak on the spectrum decreases significantly as α increases from 0° to 45°, indicating the breakdown of the vortex structures and the reduction of vortex strength.

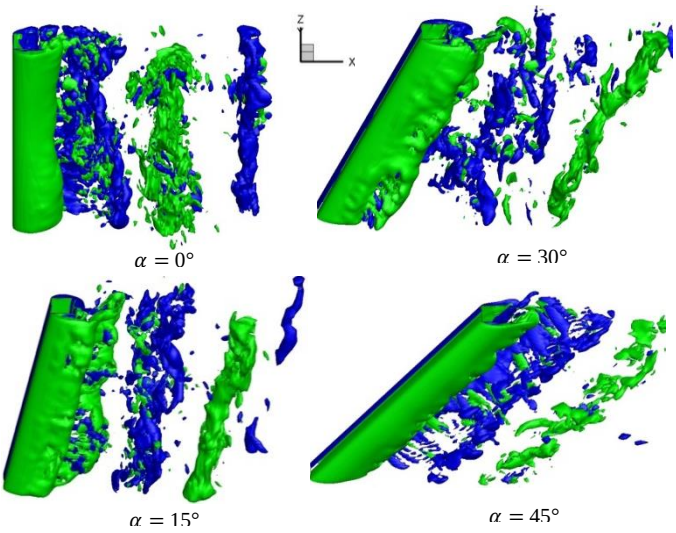

Figure 4 Spanwise vorticity iso-surfaces for different yaw angles ($|\omega_z| = 2$)

Vortex structures

The vorticity component in the spanwise directions is defined as

$$\omega_z = \frac{\partial v}{\partial x} - \frac{\partial u}{\partial y} \qquad (3)$$

u and v are the velocity component in the x and y directions, respectively. The instantaneous iso-surfaces of the spanwise vorticity ω_z at the same phase for different angles are shown in Figure 4. The (x, y)-plane has been rotated counter-clockwise by 20° with respect to the x-axis to obtain a better view of the vorticity field. The green color represents the positive iso-surfaces and the blue represents the negative ones. Overall the vortex shedding process in the square cylinder wake is not as organized as that in a circular cylinder wake at the same Reynolds number [5], which indicates a stronger interaction among the shedding vortices in the square cylinder wake. It can be seen that the separation points are fixed at the two upstream tips of the square cross-section, which is different from that of the circular cylinder with periodical oscillating separation points. At $\alpha =$ 0°, vortex dislocations can be observed even very close to the cylinder and the iso-surfaces of the spanwise vorticity become more chaotic and the size becomes smaller when the vortices propagate downstream. In Figure 4 (a), three tubes of spanwise vorticity are observed and they display relatively organized shapes until $x = 10D$. However, fewer spanwise vorticity cells are observed as α increases, and the shape of the cells become less organized, especially for $\alpha =$ 30° and 45° where the iso-contours seem to break up into smaller scale structures. The significant change in the primary spanwise vortex shedding at $\alpha =$ 30° and 45° indicates that the yaw angle has a stronger effect on the square cylinder wake than that on the circular one [5]. For each case itself, it can be noticed that the spanwise vorticity tubes show some wavy deformations along the axis. This is due to the phase difference of the pressure distribution along the cylinder

during vortex shedding. With the increase of α, the shedding of the spanwise vortices are oriented at the cylinder yaw angles, i.e. parallel to the cylinder axis, regardless of some local vortices with the disorganized shapes observed at $\alpha = 30°$ and 45°.

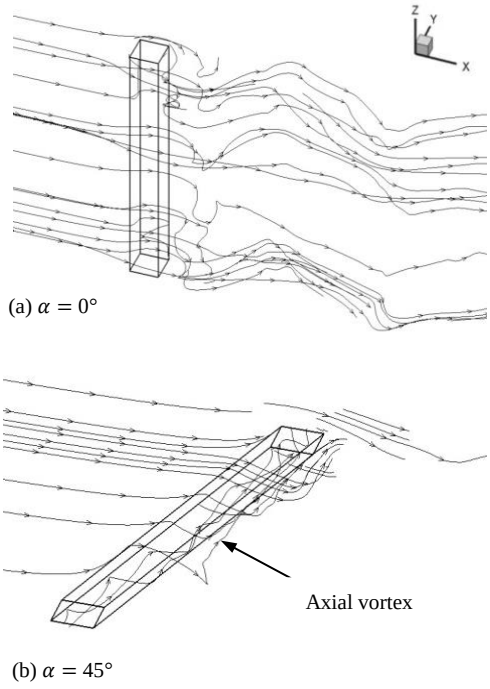

(a) $\alpha = 0°$

(b) $\alpha = 45°$

Figure 5 Schematic plots of (U, V, W) streamlines around the cylinder

In order to have a direct view of the three-dimensionality development of the wake flow, the computed three-dimensional streamlines are shown in Figure 5 for $\alpha = 0°$ and 45°. At $\alpha = 0°$, the upstream streamlines are parallel and travelling around the cylinder body to form the Kármán vortex downstream (Figure 5a). To highlight the axial velocity component at $\alpha = 45°$, only a few streamlines are plotted in Figure 5 (b). One can see that generally, when the streamlines approach the cylinder, they tend to the direction perpendicular to the cylinder axis. Immediately downstream of the cylinder, the streamlines bend to the spanwise direction for some distance, which contributes to the axial velocity as well as the axial vortex. According to [5], the spanwise bent flow is trapped in the principal spanwise vortex for some distance, and then released once the principal spanwise vorticity is shed from the cylinder surface and changes back to the incoming flow direction. Therefore the vortices right behind the cylinder body propagate in both the streamwise and the spanwise directions. This phenomenon, however, is absent for the streamlines at $\alpha = 0°$, which once again manifests the fact that the three-dimensionality of the wake is intensified by the existence of the yaw angle.

CONCLUSION

Direct numerical simulations on a square cylinder yawed with angles of 0°, 15°, 30° and 45° in steady flow are conducted to investigate the effect of the yaw angles on the wake structures. The finite volume method with OpenFOAM was applied to solve the three-dimensional Navier-Stokes equations. The main conclusions are summarized as follows.

When the velocity component normal to the cylinder axis is introduced, both the mean drag coefficient and the Strouhal number follow the IP very well (with a discrepancy of about 3%). Generally, the IP is followed better till a larger yaw angle (>45°) for the present numerical study.

The computed spanwise vortices are parallel to the cylinder axis for all yaw angles. The less organized iso-surfaces and smaller magnitude of the vorticity contours at $\alpha = 45°$ indicate the breakdown of the primary vortical structures. The streamlines in the spanwise direction of the cylinder reflects the strong spanwise velocity component in the vortex right behind the cylinder, which contributes to the three-dimensionality of the wake flow.

REFERENCES

[1] Ramberg, S.E., The effect of yaw and finite length upon the vortex wakes of stationary and vibrating circular cylinders, *Journal of Fluid Mechanics*, Vol. 128, 1983, pp. 81-107

[2] Thakur, A., Liu, X., and Marshall, J.S., Wake flow of single and multiple yawed cylinders, *Journal of Fluids Engineering*,Vol. 126, 2004, pp. 861-870

[3] Zhou, T., Wang, H., Razali, S.F., Zhou, Y., and Cheng, L., Three-dimensional vorticity measurements in the wake of a yawed circular cylinder, *Physics of Fluids*, Vol. 22, 2010, No. 015108

[4] Marshall, J.S., Wake dynamic of a yawed cylinder, *Journal of Fluids Engineering*, Vol. 125, 2003, pp. 97-103

[5] Zhao, M., Cheng, L., and Zhou, T., Direct numerical simulation of three-dimensional flow past a yawed circular cylinder of infinite length, *Journal of Fluids and Structures*, Vol. 25, 2009, pp. 831-847

[6] Lyn, D.A., Einav, S., Rodi, W., and Park, J.H., A laser-Doppler velocimetry study of ensemble-averaged characteristics of the turbulent near wake of a square cylinder, *Journal of Fluid Mechanics*, Vol. 304, 1995, pp. 285-319

[7] Saha, A.K., Biswas, G., and Muralidhar, K., Three-dimensional study of flow past a square cylinder at low Reynolds numbers, *International Journal of Heat and Fluid Flow*, Vol. 123, 2003, pp. 54-66

[8] Lou, X., Zhou, T., Wang, H. and Cheng, L., Experimental investigation on wake characteristics behind a yawed square cylinder, *Journal of Fluids and Structures*, Vol. 61, 2016, pp. 274-294

[9] Kim, D.H., Yang, K.S., and Senda, M., Large eddy simulation of turbulent flow past a square cylinder confined in a channel, *Computers & Fluids*, Vol. 33, 2004, pp. 81-96

[10] Tamura, T., Miyagi, T., and Kitagishi, T., Numerical prediction of unsteady pressures on a square cylinder with various corner shapes, *Journal of Wind Engineering and Industrial Aerodynamics*, Vol. 74-76, 1998, pp. 531-542

[11] Davis, R.W., and Moore, E.F.,, A numerical study of vortex shedding from rectangles, *Journal of Fluid Mechanics*, Vol. 116, 1982, pp. 475-506

[12] Okajima, A., Strouhal numbers of rectangular cylinders, *Journal of Fluid Mechanics*, Vol. 123, 1982, pp. 379-398

[13] Ozgoren, M., Flow structure in the downstream of square and circular cylinders, *Flow Measurement and Instrumentation*, Vol. 17, 2006, pp. 225-235